Supporting Information for "Two-dimensional particle-in-cell simulations of magnetosonic waves in the dipole magnetic field: On a constant L-shell"

Kyungguk Min[1], Kaijun Liu[2], Richard E. Denton[3], František Němec[4], Scott A. Boardsen[5,6], Yoshizumi Miyoshi[7]

[1]Department of Astronomy and Space Science, Chungnam National University, Daejeon, Korea.

[2]Department of Earth and Space Sciences, Southern University of Science and Technology, Shenzhen, China.

[3]Department of Physics and Astronomy, Dartmouth College, Hanover, New Hampshire, USA.

[4]Faculty of Mathematics and Physics, Charles University, Prague, Czech Republic.

[5]NASA/GSFC, Greenbelt, Maryland, USA.

[6]Goddard Planetary Heliophysics Institute, University of Maryland, Baltimore County, Maryland, USA.

[7]ISEE, Nagoya University, Nagoya, Japan.

Contents of this file

Additional Supporting Information (Files uploaded separately)

Corresponding author: K. Min, Department of Astronomy and Space Science, Chungnam National University, Daejeon, Korea. (kyungguk@me.com)

Introduction This supplementary material provides additional information supporting the main article.

Text S1. Model Description Some ground work for the PIC model in dipole geometry has been laid out by Min, Liu, Denton, and Boardsen (2018) and Min, Němec, Liu, Denton, and Boardsen (2019). The description of the model here is focused on the special feature of the present simulation domain on a constant L-shell surface.

S1.1 Governing Equations

Similar to other PIC codes (e.g., Liu, 2007), the equations to be solved are Maxwell's equations for the electric and magnetic fields

$$\begin{aligned} \nabla \cdot \mathbf{E} = 4\pi\rho; \qquad \nabla \times \mathbf{E} = -\frac{1}{c}\frac{\partial \mathbf{B}}{\partial t}; \\ \nabla \cdot \mathbf{B} = 0; \qquad \nabla \times \mathbf{B} = \frac{1}{c}\frac{\partial \mathbf{E}}{\partial t} + \frac{4\pi}{c}\mathbf{J}; \end{aligned} \tag{1}$$

equations of motion for kinetic particle species, α

$$m_\alpha \frac{\mathrm{d}\mathbf{v}}{\mathrm{d}t} = q_\alpha \left(\mathbf{E} + \frac{\mathbf{v}}{c} \times \mathbf{B}\right); \tag{2}$$

and the cold plasma momentum equation for the cold species, c (adopting the approach of Tao, 2014)

$$\frac{\partial \mathbf{J}_c}{\partial t} = \frac{n_c q_c^2}{m_c}\mathbf{E} + \mathbf{J}_c \times \frac{q_c}{m_c c}\mathbf{B}. \tag{3}$$

S1.2 Coordinates

We use orthogonal coordinates (ϕ, s), where ϕ denotes the usual azimuthal coordinate and $s \equiv LR_E \int_0^{\lambda_{\mathrm{lat}}} \sqrt{1 + 3\sin^2\lambda_{\mathrm{lat}}}\mathrm{d}\lambda_{\mathrm{lat}}$ is the dipole field line arc length. The grid points in the ϕ direction are regularly spaced, but in the s direction the grid point density is inversely proportional to the dipole field strength (e.g., Hu & Denton, 2009).

For two-dimensional simulations in the meridional plane (typically used in simulations of electromagnetic ion cyclotron waves (e.g., Hu & Denton, 2009) and chorus (e.g., Lu et al., 2019)), ϕ is ignorable (i.e., $\partial/\partial\phi = 0$) when solving the field equations. Likewise, for the present simulations in a constant L-shell plane, ν is assumed to be ignorable (i.e., $\partial/\partial\nu = 0$), where ν is the coordinate perpendicular to both ϕ and s. For particles, since the particles' cyclotron motion must be resolved to properly describe drift and bounce motion, all three coordinates are kept for the simulation particles.

S1.3 Equilibrium

The dipole magnetic field is curl-free ($\nabla \times \mathbf{B}_0 = 0$). When a distribution of charged particles is introduced, it generally produces a non-vanishing current. For equilibrium, an additional magnetic field $\mathbf{B}_1$ should be introduced to balance this current: $\nabla \times \mathbf{B}_1 = (4\pi/c)\mathbf{J}_{1,\perp}$. For the two-dimensional case where ϕ is ignorable, this current amounts to (e.g., Ebihara & Ejiri, 2003; Hu et al., 2010)

$$\mathbf{J}_{1,\perp} \approx c\frac{\mathbf{B}_0}{B_0^2} \times \left[\nabla P_\perp + (P_\parallel - P_\perp)\frac{(\mathbf{B}_0 \cdot \nabla)\mathbf{B}_0}{B_0^2}\right], \tag{4}$$

where $P_\perp$ and $P_\parallel$ are the pressure components perpendicular and parallel to $\mathbf{B}_0$, respectively. Note that the total magnetic field $\mathbf{B}$ is replaced by $\mathbf{B}_0$, assuming $B_1 \ll B_0$.

For the present setup, the expression for $\mathbf{J}_{1,\perp}$ is different. For a distribution, f, of charged particles, the current density is given by

$$\mathbf{J}_{1,\perp} = q\int (\mathbf{V}_{GC} + \mathbf{v}_g) f \mathrm{d}^3 v, \tag{5}$$

where we have separated the velocity, $\mathbf{v}$, into the guiding center part, $\mathbf{V}_{GC}$, and the gyrating part, $\mathbf{v}_g$. Making use of the expression for the velocity of the guiding center (e.g., Roederer, 1970) located at L_0, the current density due to guiding center motion may be written as

$$\mathbf{J}_{GC} = \frac{c}{B}\frac{\mathbf{B} \times \nabla B}{B^2}\left(P_\perp + P_\parallel\right). \tag{6}$$

Considering the diagram shown in Figure S2, the contribution to $\mathbf{J}_{1,\perp}$ due to gyration comes from the fact that with azimuthal symmetry, the arc length of the inbound and outbound portions of the gyro orbit separated by the constant-L_0 surface is different. As a result, $\langle \mathbf{v}_g \cdot \mathbf{e}_\phi \rangle$ is non-vanishing, where the angled brackets denote gyro-averaging. (On the other hand, $\langle \mathbf{v}_g \cdot \nabla L \rangle$ vanishes due to symmetry.) To quantify this contribution for dipole geometry, let us consider the coordinate system shown in Figure S3. (The x axis is along the Earth's dipole moment.) The guiding center position in the unprimed coordinate system is given by $\mathbf{R} = R(\sin\lambda \mathbf{e}_x + \cos\lambda \mathbf{e}_y)$. For a gyro-radius, r_g, much smaller than R, the gyro-velocity vector may be written as

$$\begin{aligned} \mathbf{v}_g &= v_\perp \left(\mathbf{e}_{y'} \cos(\Omega_c t) - \mathbf{e}_z \sin(\Omega_c t) \right) \\ &= v_\perp \left[\mathbf{e}_x \cos(\Omega_c t) \frac{3\xi\sqrt{1-\xi^2}}{\sqrt{1+3\xi^2}} + \mathbf{e}_y \cos(\Omega_c t) \frac{1-3\xi^2}{\sqrt{1+3\xi^2}} - \mathbf{e}_z \sin(\Omega_c t) \right], \end{aligned} \tag{7}$$

where Ω_c is the (signed) cyclotron frequency (evaluated at the guiding center); $v_\perp = |\mathbf{v}_g|$; $\xi = \sin\lambda$; and

$$\mathbf{e}_{x'} = \frac{1-3\xi^2}{\sqrt{1+3\xi^2}} \mathbf{e}_x - \frac{3\xi\sqrt{1-\xi^2}}{\sqrt{1+3\xi^2}} \mathbf{e}_y \text{ and } \mathbf{e}_{y'} = \frac{3\xi\sqrt{1-\xi^2}}{\sqrt{1+3\xi^2}} \mathbf{e}_x + \frac{1-3\xi^2}{\sqrt{1+3\xi^2}} \mathbf{e}_y. \tag{8}$$

Making use of the expression for the gyro-radius vector

$$\mathbf{r}_g = \frac{\mathbf{B} \times \mathbf{v}_g}{B\Omega_c} = r_g \left(\mathbf{e}_{y'} \sin(\Omega_c t) + \mathbf{e}_z \cos(\Omega_c t) \right), \tag{9}$$

the position vector of the particle is written as

$$\begin{aligned} \mathbf{r} &= \mathbf{R} + \mathbf{r}_g \\ &= \left(R\xi + r_g \sin(\Omega_c t) \frac{3\xi\sqrt{1-\xi^2}}{\sqrt{1+3\xi^2}} \right) \mathbf{e}_x + \left(R\sqrt{1-\xi^2} + r_g \sin(\Omega_c t) \frac{1-3\xi^2}{\sqrt{1+3\xi^2}} \right) \mathbf{e}_y \\ &\quad + r_g \cos(\Omega_c t) \mathbf{e}_z. \end{aligned} \tag{10}$$

Meanwhile, with the position vector $\mathbf{r} = r_x\mathbf{e}_x + r_y\mathbf{e}_y + r_z\mathbf{e}_z$ and $\mathbf{r}\cdot\mathbf{e}_\phi = 0$, the unit vector in the azimuthal direction at the particle position can be written as

$$\mathbf{e}_\phi(\mathbf{r}) = \frac{-r_z\mathbf{e}_y + r_y\mathbf{e}_z}{\sqrt{r_y^2 + r_z^2}}. \tag{11}$$

Using equation (10), the denominator can be written as

$$\begin{aligned} r_y^2 + r_z^2 &= \left(R\sqrt{1-\xi^2} + r_g\sin(\Omega_c t)\frac{1-3\xi^2}{\sqrt{1+3\xi^2}}\right)^2 + r_g^2\cos^2(\Omega_c t) \\ &\approx R^2\left((1-\xi^2) + 2\frac{r_g}{R}\sin(\Omega_c t)(1-3\xi^2)\frac{\sqrt{1-\xi^2}}{\sqrt{1+3\xi^2}}\right), \end{aligned} \tag{12}$$

where $r_g/R \ll 1$ is assumed for the approximate expression. Finally, combining equations (10), (11), and (12), the azimuthal component of the gyro velocity can be written as

$$\begin{aligned} \mathbf{v}_g\cdot\mathbf{e}_\phi &= \frac{-v_\perp}{\sqrt{(1-\xi^2) + 2\frac{r_g}{R}\sin(\Omega_c t)(1-3\xi^2)\frac{\sqrt{1-\xi^2}}{\sqrt{1+3\xi^2}}}}\left(\sqrt{1-\xi^2}\sin(\Omega_c t) + \frac{r_g}{R}\frac{1-3\xi^2}{\sqrt{1+3\xi^2}}\right) \\ &\approx -v_\perp\left(\sin(\Omega_c t) + \frac{r_g}{R\sqrt{1-\xi^2}}\frac{1-3\xi^2}{\sqrt{1+3\xi^2}}\cos^2(\Omega_c t)\right), \end{aligned} \tag{13}$$

where $r_g/R \ll 1$ is assumed for the approximate expression. Gyro-averaging $\mathbf{v}_g\cdot\mathbf{e}_\phi$ yields

$$\langle\mathbf{v}_g\cdot\mathbf{e}_\phi\rangle \approx -\frac{v_\perp^2}{2\Omega_c R}\frac{1-3\xi^2}{\sqrt{(1-\xi^2)(1+3\xi^2)}}. \tag{14}$$

Finally, evaluation of $\mathbf{J}_g = q\int\langle\mathbf{v}_g\rangle f\mathrm{d}^3v$ yields the gyro-averaged current density due to gyro-motion

$$\mathbf{J}_g \approx -\mathbf{e}_\phi\frac{1-3\xi^2}{\sqrt{(1-\xi^2)(1+3\xi^2)}}\frac{c}{B}\frac{P_\perp}{R}. \tag{15}$$

Combining equations (6) and (15), the total current density is given by

$$\mathbf{J}_{1,\perp} = \frac{c}{B}\frac{\mathbf{B}\times\nabla B}{B^2}\left(P_\perp + P_\parallel\right) - \mathbf{e}_\phi\frac{c}{B}\frac{1-3\xi^2}{\sqrt{(1-\xi^2)(1+3\xi^2)}}\frac{P_\perp}{R}. \tag{16}$$

Figure S4 compares the above analytic expression and the result from test particle tracing.

Captions for Movies S8 to S11 Movies S8 and S9 show the movie version of Figure 4b, corresponding to $\delta B_\parallel$ and δE_ϕ, respectively.

Movies S10 and S11 show the movie version of Figure 7, corresponding to $\delta B_{\parallel}$ and δE_{ϕ}, respectively.

References

Ebihara, Y., & Ejiri, M. (2003, January). Numerical Simulation of the Ring Current: Review. *Space Sci. Rev.*, *105*, 377-452. doi: 10.1023/A:1023905607888

Hu, Y., & Denton, R. E. (2009, December). Two-dimensional hybrid code simulation of electromagnetic ion cyclotron waves in a dipole magnetic field. *Journal of Geophysical Research (Space Physics)*, *114*, A12217. doi: 10.1029/2009JA014570

Hu, Y., Denton, R. E., & Johnson, J. R. (2010, September). Two-dimensional hybrid code simulation of electromagnetic ion cyclotron waves of multi-ion plasmas in a dipole magnetic field. *Journal of Geophysical Research (Space Physics)*, *115*, A09218. doi: 10.1029/2009JA015158

Liu, K. (2007). *Particle-in-cell simulations of particle energization in the auroral region* (Unpublished doctoral dissertation). Cornell University.

Lu, Q., Ke, Y., Wang, X., Liu, K., Gao, X., Chen, L., & Wang, S. (2019, Jun). Two-Dimensional gcPIC Simulation of Rising-Tone Chorus Waves in a Dipole Magnetic Field. *Journal of Geophysical Research (Space Physics)*, *124*(6), 4157-4167. doi: 10.1029/2019JA026586

Min, K., & Liu, K. (2020). Linear Instability and Saturation Characteristics of Magnetosonic Waves along the Magnetic Field Line. *Journal of Astronomy and Space Sciences*, *37*, 85-94. Retrieved from `http://janss.kr/journal/article.php?code=73141` doi: https://doi.org/10.5140/JASS.2020.37.2.85

Min, K., Liu, K., Denton, R. E., & Boardsen, S. A. (2018, September). Particle-in-

Cell Simulations of the Fast Magnetosonic Mode in a Dipole Magnetic Field: 1-D Along the Radial Direction. *Journal of Geophysical Research (Space Physics)*, *123*, 7424-7440. doi: 10.1029/2018JA025666

Min, K., Němec, F., Liu, K., Denton, R. E., & Boardsen, S. A. (2019, Jun). Equatorial Propagation of the Magnetosonic Mode Across the Plasmapause: 2-D PIC Simulations. *Journal of Geophysical Research (Space Physics)*, *124*(6), 4424-4444. doi: 10.1029/2019JA026567

Roederer, J. G. (1970). *Dynamics of geomagnetically trapped radiation.* (Physics and Chemistry in Space, Berlin: Springer, 1970)

Tao, X. (2014, May). A numerical study of chorus generation and the related variation of wave intensity using the DAWN code. *Journal of Geophysical Research (Space Physics)*, *119*, 3362-3372. doi: 10.1002/2014JA019820

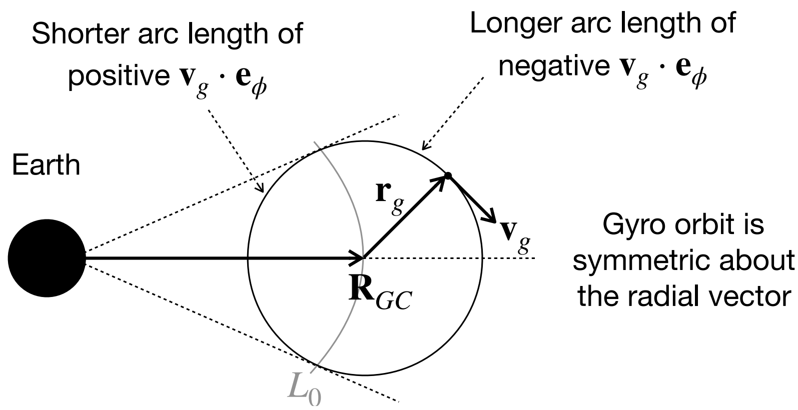

Figure S2. An illustration of the finite gyro-radius contribution to the current density.

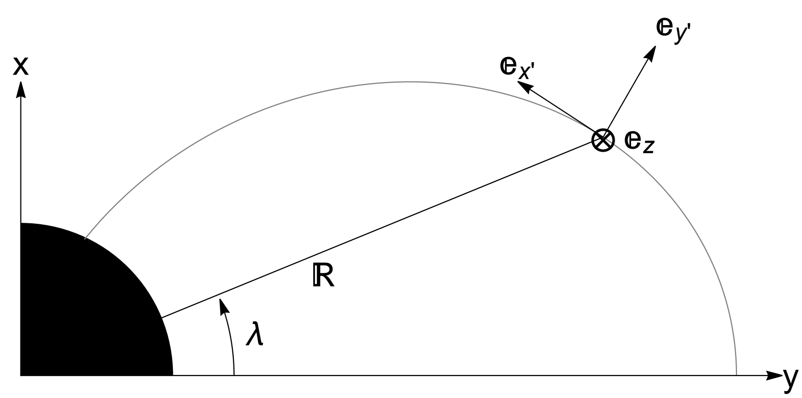

Figure S3. The coordinates (x, y, z) are defined in the Earth-centered Cartesian coordinate system whose x-y plane contains the guiding center, $\mathbf{R}$. (The x axis is along the Earth's dipole moment.) The coordinates (x', y', z') are defined in the local Cartesian coordinate system centered at the guiding center, $\mathbf{R}$, as depicted. Here, $\mathbf{e}_z = \mathbf{e}_{z'}$.

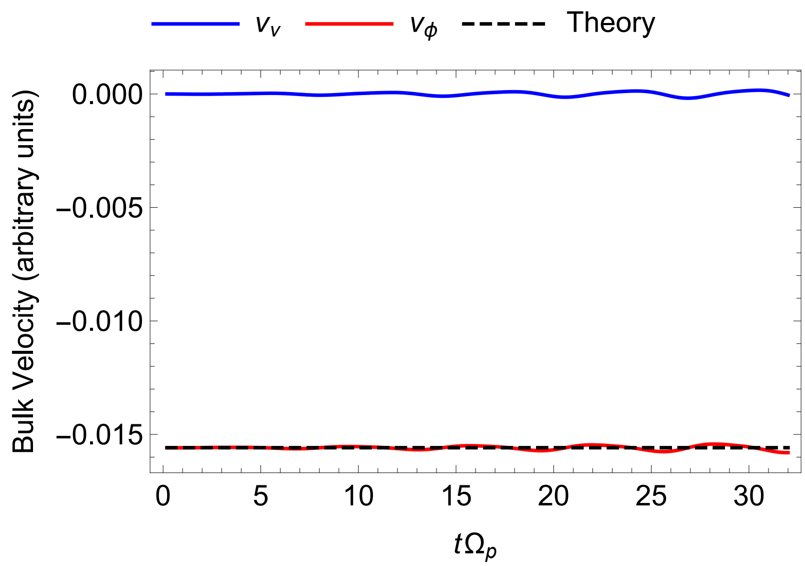

Figure S4. Time evolution of the average velocity of equatorially mirroring test particles initialized according to the delta function distribution, $f \sim \delta(v_\parallel)\delta(v_\perp - v_r)$. The blue curve represents the radial (ν) component which has zero average value. The red curve represents the azimuthal component which is negative for positively-charged particles. The dashed line denotes the value obtained using equation (16).

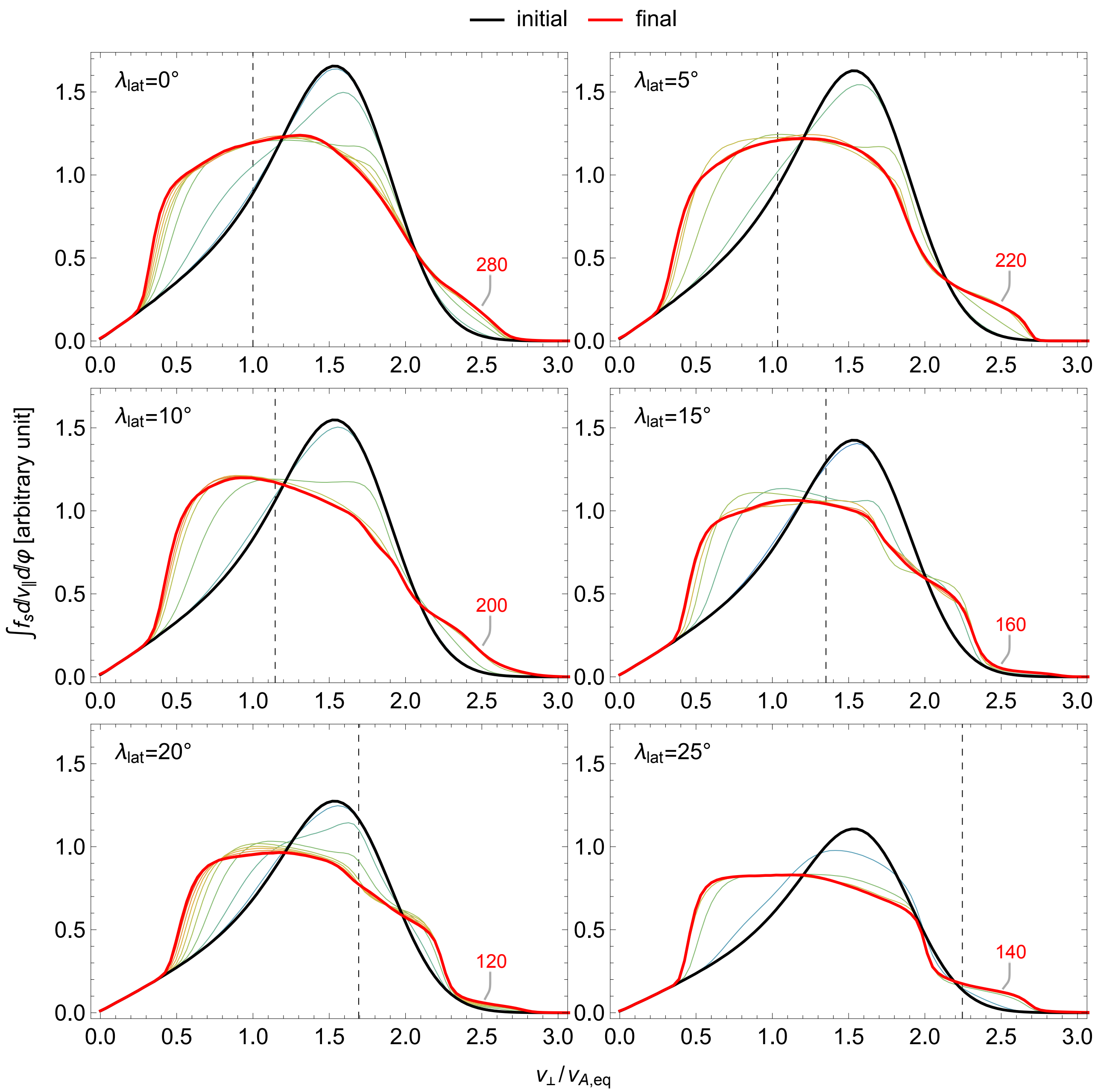

Figure S5. Time evolution of the reduced velocity distributions ($\iint f dv_{\|} d\phi$) of partial shell protons sampled at the latitude listed in each panel. These results are from the local two-dimensional PIC simulations carried out by Min and Liu (2020). Colors from black to red represent the progression of simulation time with the end time labeled in each panel. The vertical dashed lines denote $v_A(\lambda_{\rm lat})/v_{A,\rm eq}$.

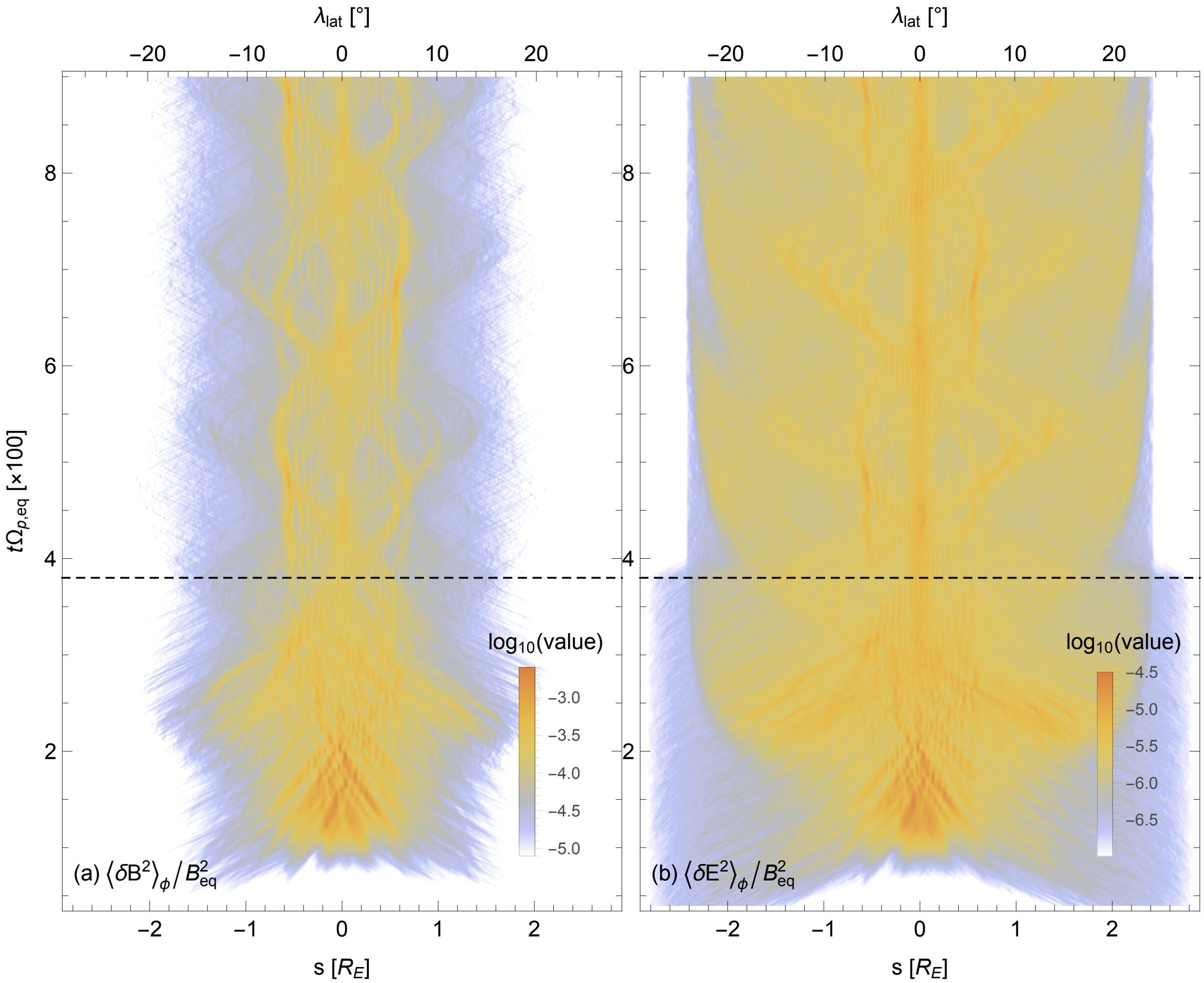

Figure S6. Two-dimensional color plots (in logarithmic scale) of (a) magnetic, $\langle \delta B^2 \rangle_\phi$, and (b) electric, $\langle \delta E^2 \rangle_\phi$, field intensity corresponding to Figures 5a and 5b in the main article but for the simulation with an extended time period. The horizontal dashed lines denote the time when all kinetic particles were removed from the system.

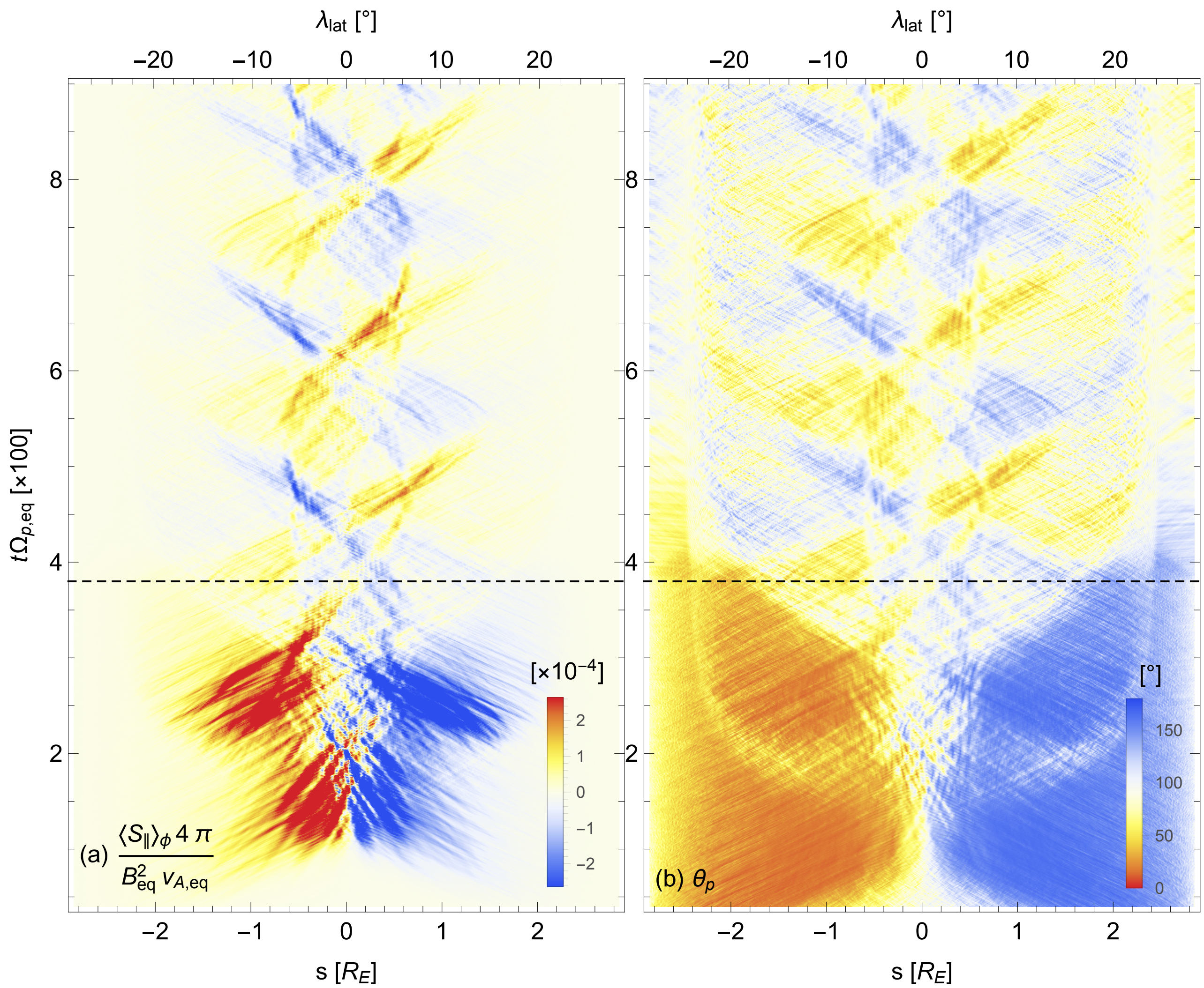

Figure S7. (a) Parallel component of the Poynting flux, $\langle S_\parallel \rangle_\phi$, shown in linear scale corresponding to Figure 5c but for the simulation with an extended time period. (b) Poynting vector angle, $\theta_p = \cos^{-1}(\langle S_\parallel \rangle_\phi / \langle |\mathbf{S}| \rangle_\phi)$, corresponding to Figure 5d but for the simulation with an extended time period. The horizontal dashed lines denote the time when all kinetic particles were removed from the system.